Electrochimica Acta 391 (2021) 138916

Contents lists available at ScienceDirect

Electrochimica Acta

journal homepage: www.elsevier.com/locate/electacta

On the stabilization and extension of the distribution of relaxation times analysis

Davide Clematis[a,1,*], Tommaso Ferrari[b,1], Antonio Bertei[b,*], Antonio Maria Asensio[a], Maria Paola Carpanese[a,c], Cristiano Nicolella[b], Antonio Barbucci[a,c]

[a] Department of Civil, Chemical and Environmental Engineering (DICCA), University of Genoa, Via all'Opera Pia 15, Genova 16145, Italy
[b] Department of Civil and Industrial Engineering (DICI), University of Pisa, Largo Lucio Lazzarino 2, Pisa 56126, Italy
[c] Institute of Condensed Matter Chemistry and Technology for Energy, National Research Council (CNR-ICMATE), Via De Marini 6, Genova 16149, Italy

ARTICLE INFO

Article history:
Received 21 June 2021
Accepted 9 July 2021
Available online 16 July 2021

Keywords:
Electrochemical impedance spectroscopy
Distribution of relaxation times
Tikhonov regularization
Zero-padding
Electrochemical characterisation

ABSTRACT

The Distribution of Relaxation Times (DRT) is a useful technique to provide an improved insight into the interpretation of Electrochemical Impedance Spectroscopy (EIS) data. Despite its capability to distinguish the characteristic frequencies of the processes involved in an electrochemical system, the DRT solution is an ill-posed problem that requires a regularization method. Tikhonov regularization is one of the most commonly adopted methods for DRT analysis. Nevertheless, the domain discretization, needed to solve the original continuous problem, introduces errors in DRT evaluation. This problem is quite relevant when the impedance is not sufficiently resolved at boundary frequency range (imaginary part of impedance does not approach 0), affecting the edges of the DRT spectrum and the internal part. Here, the zero-padding technique is applied to overcome this issue. The results show how this approach, frequently used in the signal theory but not in DRT, improves DRT evaluation quality with Tikhonov regularization. It consists of an extension of the experimental frequency domain, reducing the errors due to the frequency truncation. The extended algorithm, named ED-DRT, is compared with the conventional Tikhonov method on both simulated and real impedance data. The new approach increases the quality of DRT results, providing higher stability and accuracy in evaluating characteristic frequencies and global polarization resistance even with noisy EIS data.

1. Introduction

Electrochemical Impedance Spectroscopy (EIS) is one of the tools available to investigate electrochemical processes and materials behaviour under real operating conditions. It can provide several helpful information for characterization, diagnosis and optimization [1–4]. EIS relies on the interrogation of the electrochemical system *via* perturbation with a sinusoidal input (e.g., the current) and detection of the output (e.g., the voltage, or vice versa), repeated for different frequencies. After transforming the signals in complex variables *via* Fourier transform, the ratio between voltage and current gives the impedance of the system. The impedance data, typically collected over a range of frequencies spanning several orders of magnitude, represent the basis for identification and separation of the elementary processes according to their characteristic time constant.

Thanks to the friendly instrumental interfaces, EIS has gained great popularity in scientific communities and also in the industry. However, interpretation of impedance data needs accurate analysis. It should also be mentioned that any attempt to investigate impedance data should rely on measurements free of artefacts and on measurement strategies designed to simplify the overall system and possibly separate individual process contributions (inductance correction, half-cell configuration [5–7]).

Nowadays, equivalent circuit modelling [8–10] and physically-based models [11–18] are the most reliable EIS interpretation approaches. The former is based on a description of the system using electrical components, each characterized by a physical meaning. To increase the accuracy in the process description, extra elements have been added to the conventional elements (capacitor C, resistor R and inductor I): they are known as constant phase element (CPE) [19,20], Warburg (W) and Gerischer (Ge) elements, which take into account surface heterogeneities, chemical and electrochemical reactions and diffusive processes [8,9,21–25]. Equivalent

* Corresponding authors.
E-mail addresses: davide.clematis@edu.unige.it (D. Clematis), antonio.bertei@unipi.it (A. Bertei).
[1] These authors contributed equally to this work

https://doi.org/10.1016/j.electacta.2021.138916
0013-4686/

circuit modelling allows for the extrapolation of many process parameters, but the definition a priori of the number of circuit elements and their relationship with the real physical phenomena are not trivial tasks [26,27]. To go deeper inside into the mechanistic interpretation, physically-based models have been developed to determine, *via* EIS simulations, material properties and factors which influence system performance. One of the strengths of modelling is the possibility to investigate the system at different length and time scales, from surface chemistry (phenomena at nano-scale) to system scale (meter/years) and the integration among these scale levels [28,29].

Nevertheless, in order to allow EIS interpretation, both approaches need preliminary hypotheses about the number of elements to include in the equivalent circuit or the number of physical phenomena that the model must take into account. This preliminary step is often very crucial since the correct identification of the number of physical processes in EIS can avoid over-fitting of data as well as possible errors and misattributions in EIS interpretation. In the last years, the distribution of relaxation times (DRT) has been introduced as a further methodology to analyze EIS data [30–44]. This approach does not require any a priori knowledge regarding the processes involved. As such, DRT allows for the separation of the characteristic frequency of each impedance contribution of the electrochemical system [11,45].

Broadly speaking, at the basis of the DRT approach there is an infinite series of RC elements having time constants spanning the whole frequency range, from zero to infinite. The DRT seeks to retro-fit the resistance value of each RC element (i.e., the weights of the distribution function) from the measured EIS data. However, mathematically speaking, retro-fitting the theoretically infinite number of weights of the distribution function from a finite number of EIS data is an ill-posed problem that requires a proper regularization method [46]. Significant contributions in the investigation of DRT and how to stabilize its solution have been published in the last years [32,34,37,46,47]; among the different approaches, the Tikhonov regularization method stands out as the most classical and commonly used one [30,32,37,48]. Previous studies also reported that DRT can suffer from the possible formation of artefacts such as additional spurious peaks and divergence from the expected solution in some critical situations [46,49]. Although possible solutions have been proposed, most of them, to the best of authors knowledge, require or have been applied to a complete EIS spectrum, which means that the imaginary part of impedance must be sufficiently close to zero at both high and low frequencies to resolve the arcs completely. Therefore, what it is currently missing is a systematic investigation of the stability of DRT when the impedance data does not intercept the real-impedance axis in the Nyquist plot at the frequency bounds. This is a frequent situation occurring when the collection of low-frequency EIS data is time-consuming, if not even impossible, because the system evolves/degrades during the measurement, as well as at high frequency when subtraction of wires inductance is performed.

In this study, a discussion about the effect of incomplete EIS spectra on DRT analysis is carried out by comparing the common Tikhonov regularization with a new simple variation proposed here and named Extended Domain Distribution of Relaxation Time (ED-DRT), which is based on the extension of the frequency domain over the sampling data collection. In the first part of the study, the algorithms are used to analyze synthetic data obtained from equivalent circuit simulation. The effect of the density of points per decade and the effect of noise are presented and discussed. In the second section of the paper, the ED-DRT approach is tested on real measurements of symmetrical solid oxide cells. The general conclusions of the study are summarized in the last section.

2. Theory and model description

2.1. Tikhonov regularization

The concept behind the DRT is the representation of complex impedance data $Z(\omega_k)$ as an infinite series of RC-elements through deconvolution from the frequency domain to time domain [33,50], as reported by Eq. (1):

$$Z(\omega_k) = R_0 + R_p \int_0^{\infty} \frac{H(\tau)}{1 + i\omega_k\tau} d\tau \tag{1}$$

where R_0 is the high-frequency cutoff resistance, R_P is the polarization resistance, while the integrand is the expression of the resistor//capacitance circuit defined by a characteristic time $\tau = RC$. In addition, ω_k represents the experimental sampling angular frequency, i is the imaginary unit, and $H(\tau)$ is the distribution function of relaxation times (units: s^{-1}), often identified with the acronym DRT, which satisfies the property:

$$\int_0^{+\infty} H(\tau) d\tau = 1 \tag{2}$$

so that the term $H(\tau)$ represents the weight (i.e., the "density contribution") of the RC circuit with time constant τ.

In this analysis, only the imaginary part of the EIS spectra is considered. It is possible to make this assumption without losing information due to the Kramers-Kronig relation, making the imaginary and real part of the impedance interdependent [50,51]. Then, Eq. (1) reduces to:

$$Z_{Im}(\omega_k) = -R_p \int_0^{+\infty} H(\tau) \frac{\omega_k\tau}{1 + (\omega_k\tau)^2} d\tau \tag{3}$$

Operating a proper variable manipulation Eq. (3) assumes the following form:

$$\begin{aligned} Z_{Im}(\omega_k) &= -R_p \int_0^{+\infty} H(\tau)\tau \frac{\omega_k\tau}{1 + (\omega_k\tau)^2} \frac{d\tau}{\tau} \\ &= -R_p \int_{-\infty}^{+\infty} G(\tau) \frac{\omega_k\tau}{1 + (\omega_k\tau)^2} d\ln\tau \end{aligned} \tag{4}$$

having considered that the extremes of the integration correspond to $\tau = 0 \rightarrow \ln\tau = -\infty$, $\tau = +\infty \rightarrow \ln\tau = +\infty$, and having defined the density distribution function $G(\tau) = H(\tau)\cdot\ \tau > 0$ (units: dimensionless), which enables integration in logarithmic space with property:

$$\int_{-\infty}^{+\infty} G(\tau) d\ln\tau = 1 \tag{5}$$

Since the objective of DRT is the identification of the distribution function $G(\tau)$, instead of spanning the whole range of time constants τ from 0 to $+\infty$, it is reasonable to bound the search within $\tau_{min} \le \tau \le \tau_{max}$, where τ_{min} and τ_{max} indicate the lower and upper bounds of time constants we are looking for [52]. Note that such a range $\tau_{min} \le \tau \le \tau_{max}$ can even be larger than the range of frequencies measured experimentally and for which we want to reconstruct $Z_{Im}(\omega_k)$. In such a case, Eq. (4) can be approximated as:

$$Z_{Im}(\omega_k) \approx -R_p \int_{\ln\tau_{min}}^{\ln\tau_{max}} G(\tau) \frac{\omega_k\tau}{1 + (\omega_k\tau)^2} d\ln\tau \tag{6}$$

We can now operate a variable change: instead of considering the time constant τ of the RC element, let us consider its characteristic angular frequency $\omega = \tau^{-1}$. It is crucial not to confuse the frequency sampled by impedance, ω_k, with the characteristic frequency of the RC element, ω, because they are two different variables. This variable change implies a change in the differential ($d\ln\tau = -d\ln\omega$), and in the extremes of integration $\ln\tau_{max} \to \ln\omega_{min}$, $\ln\tau_{min} \to \ln\omega_{max}$, where $\omega_{min} = \tau_{max}^{-1}$ and $\omega_{max} = \tau_{min}^{-1}$, so that Eq. (6) becomes:

$$Z_{Im}(\omega_k) = -R_p \int_{\ln\omega_{min}}^{\ln\omega_{max}} G(\omega) \frac{\frac{\omega_k}{\omega}}{1+\left(\frac{\omega_k}{\omega}\right)^2} d\ln\omega \tag{7}$$

Now, the angular frequency ω can be rescaled in a dimensionless form $\tilde{\omega} = \omega/\omega_{min}$. This leads to a new change in integral components, with differential $d\ln\omega = d\ln\tilde{\omega}$ and extremes of integration $\ln\omega_{min} \to \ln\tilde{\omega}_{min} = \ln\frac{\omega_{min}}{\omega_{min}} = 0$, $\ln\omega_{max} \to \ln\tilde{\omega}_{max} = \ln\frac{\omega_{max}}{\omega_{min}}$. In addition, the logarithmic scale can be changed to base 10, which is commonly used to plot impedance data, leading to:

$$Z_{Im}(\omega_k) = -R_p \int_{0}^{\log_{10}\frac{\omega_{max}}{\omega_{min}}} G(\tilde{\omega}) \frac{\frac{\omega_k}{\omega_{min}\tilde{\omega}}}{1+\left(\frac{\omega_k}{\omega_{min}\tilde{\omega}}\right)^2} \ln 10 d\log_{10}\tilde{\omega} \tag{8}$$

The integration in Eq. (8) can be approximated by using a quadrature formula by considering M log-spaced dimensionless frequency points (i.e., M–1 equal intervals) in the form $\log_{10}\tilde{\omega}_j$: $0,\ \Delta\varepsilon, 2\Delta\varepsilon, \ldots, (M-1)\Delta\varepsilon$, with $\Delta\varepsilon = (\log_{10}\frac{\omega_{max}}{\omega_{min}})/(M-1)$ denoting the log-spaced frequency interval (i.e., $\Delta\varepsilon = \Delta\log_{10}\tilde{\omega}$). By introducing the compact notation $\log_{10}\tilde{\omega}_j = j\cdot\Delta\varepsilon$ with j = *0,1...,M-1*, where $\tilde{\omega}_j = 10^{j\Delta\varepsilon}$ and $G_j = G(\tilde{\omega}_j)$, Eq. (8) is discretized as a summation with unitary quadrature coefficients as follows:

$$Z_{Im}(\omega_k) = \sum_{j=0}^{M-1} -\frac{\frac{\omega_k}{\omega_{min}\cdot 10^{j\Delta\varepsilon}}}{1+\left(\frac{\omega_k}{\omega_{min}\cdot 10^{j\Delta\varepsilon}}\right)^2} R_p G_j \ln 10\Delta\varepsilon \tag{9}$$

Eq. (9) is valid for a generic number N of experimental impedance points ω_k (i.e., *k=0,1,...,N-1*); thus, Eq. (9) can be organised in matrix form as a linear system, as follows:

$$\boldsymbol{A\rho}=\boldsymbol{Z_{Im}} \tag{10}$$

whose elements are:

$$A_{kj}=-\frac{\frac{\omega_k}{\omega_{min}\cdot 10^{j\Delta\varepsilon}}}{1+\left(\frac{\omega_k}{\omega_{min}\cdot 10^{j\Delta\varepsilon}}\right)^2},\ \rho_j = R_p G_j \ln 10\Delta\varepsilon \text{with} \sum_{j=0}^{M-1}\rho_j = R_p \tag{11}$$

Notably, in the linear system $\boldsymbol{A\rho} = \boldsymbol{Z_{Im}}$, $\boldsymbol{A}$ is a $N \times M$ matrix with elements A_{kj}, $\boldsymbol{\rho}$ is a vector of size $M \times 1$ containing the M unknown values of the distribution function G_j, and $\boldsymbol{Z_{Im}}$ is a vector of size $N \times 1$ containing the N known impedance experimental data points $Z_{Im}(\omega_k)$.

As introduced before, the resolution of such a linear system is often an ill-posed problem due to its discretization [53]. For such a reason, a regularization method is necessary to substitute the starting ill-posed linear problem with a closely-related system less sensitive to perturbations. In this context, the Tikhonov regularization method has emerged as one of the techniques more frequently used. In Tikhonov regularization the system solution must satisfy the following minimization problem:

$$\min\ \left\{\|\boldsymbol{A\rho} - \boldsymbol{Z_{Im}}\|^2 + \|\lambda\boldsymbol{\rho}\|^2\right\} \tag{12}$$

where the term $\|\lambda\boldsymbol{\rho}\|^2$ represents the regularization term, which contains the regularization parameter λ (with $\lambda > 0$), a crucial factor in calculating a reliable DRT [47,54,55], and the term $\boldsymbol{\rho}$ representing the distribution of relaxation time evaluated in the discretization points chosen for the analysis. In this study, the optimized regularization parameter λ_{sol} is obtained using the compact singular value decomposition and then the L-curve method routine provided by Hansen [56], while Eq. (12) is solved with the non-negative linear least-squares solver lsqnonneg in Matlab®, which ensures that $\rho_j \geq 0$.

2.2. Zero padding for extension of the frequency domain

In DRT analysis, it is customary to solve the linear system in Eq. (10) for N equally log-spaced experimental impedance data. By choosing the lower and upper bounds $\omega_{\min}$ and $\omega_{\max}$ of the RC circuit coincident with the minimum and maximum frequency of the sampled experimental impedance data and by using as a logarithmic frequency interval $\Delta\varepsilon$ the same interval of the N experimental impedance points, the number of unknowns ρ_j is equal to N (i.e., $M = N$) and the linear system in Eq. (10) becomes a quadratic system $N \times N$. In addition, the matrix $\mathbf{A}$ becomes a symmetric Toeplitz matrix [57] of the form:

$$\boldsymbol{A} = -\begin{bmatrix} a_1 & a_2 & a_3 & \cdots & a_N \\ a_2 & a_1 & a_2 & \cdots & a_{N-1} \\ a_3 & a_2 & a_1 & \cdots & a_{N-2} \\ \vdots & \vdots & \vdots & \ddots & \vdots \\ a_N & a_{N-1} & a_{N-2} & \cdots & a_1 \end{bmatrix} \text{with}\ \ a_j > a_{j+1} \tag{13}$$

which contains only N independent elements a_j.

However, we must recall that the system in Eq. (10) and the corresponding matrix $\mathbf{A}$ in Eq. (13) are just a discretized version, with a finite number of elements confined within $[\log_{10}\omega_{\min}, \log_{10}\omega_{\max}]$, of the continuous inversion problem with unbounded frequency ranges as originally reported in Eq. (4). In other words, the finite matrix $\mathbf{A}$ in Eqs. (11) and (13) represents only a portion of the true infinite matrix $\mathbf{A}_\infty$, spanning the whole log-spaced frequency range $(-\infty, +\infty)$, and centred at the characteristic frequency $\omega_{\min}$ of the minimum low-frequency process that we want to deconvolve with the DRT, as reported in Eq. (14):

$$\boldsymbol{A}_\infty\boldsymbol{\rho}_\infty = \boldsymbol{Z_{Im}} \text{ i.e., } \sum_{j=-\infty}^{j=+\infty} -\frac{\frac{\omega_k}{\omega_{min}\,10^{j\Delta\varepsilon}}}{1+\left(\frac{\omega_k}{\omega_{min}\,10^{j\Delta\varepsilon}}\right)^2}\cdot R_p G_j \ln 10\Delta\varepsilon = Z_{Im}(\omega_k) \tag{14}$$

Such a true infinite matrix $\mathbf{A}_\infty$, which would allow calculating the exact density distribution function $\boldsymbol{\rho}_\infty$, is a circulant matrix [57,58]. It is worth noting that, being $\mathbf{A}_\infty$ a circulant matrix, the exact linear system in Eq. (14) represents a circular convolution. Thanks to the circular convolution theorem, it can be solved using the discrete Fourier transform [58], as done by researchers who frame the original Eq. (4) as a convolution problem and solve for the DRT by using the Fourier transform [33,41,50]. Nevertheless, in any case, having discretised the exact infinite system in Eq. (14), and having restricted its bounds to the finite linear system in Eqs. (10) and (11), necessarily introduces errors in the evaluation of the DRT function, i.e., in the unknown values ρ_j of the finite vector $\boldsymbol{\rho}$.

The specific nature of the finite matrix $\boldsymbol{A}$ in Eqs. (11) and (13) makes the discretization errors quite significant, especially if the impedance is not sufficiently resolved at high or low frequencies (i.e., if $Z_{Im}(\omega_k)$ does not approach 0 for $k = 0$ or $k = N$–*1*). The truncation of the frequency range introduces errors in the evaluation of the DRT vector $\boldsymbol{\rho}$ at the edges of its spectrum (i.e., for $j \approx 0$ and $j \approx N$–1), and it can affect the internal ρ_j values (i.e., for $0 < j < N-1$). In fact, it is worth noting that the matrix $\mathbf{A}$, being it a symmetric Toeplitz matrix, operates a frequency

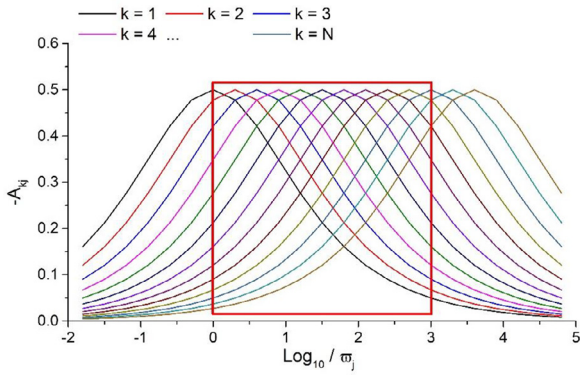

Fig. 1. Graphical representation of kernel translation of the elements of matrix ***A***. Each curve represents a row of matrix ***A*** and the part inside the red square is the portion considered in the truncated frequency range. (For interpretation of the references to color in this figure legend, the reader is referred to the web version of this article).

shift from one row to the other. In other words, the row vector $[a_1, a_2, a_3, \ldots, a_N]$, which is just a finite portion of the infinite row vector $[\ldots, a_N, \ldots, a_3, a_2, a_1, a_2, a_3, \ldots, a_N, \ldots]$ of the infinite matrix $\mathbf{A}_\infty$, shifts the elements a_j of one column at every row in the matrix **A** (see Eq. (13)). Fig. 1 graphically describes this concept: here, each curve corresponds to a row of the matrix **A**, and the red box delimits the portion considered with the truncation.

During the solution of the linear system in Eq. (10), such a frequency shift propagates the edge effects introduced by the finite frequency range even in the evaluation of the internal unknown ρ_j values [59]. Hence, not only the external values of the unknown vector $\boldsymbol{\rho}$ are affected, but auto-correlation artefacts skew the whole DRT.

The problem just described regarding the finiteness of the sampled frequency range in the deconvolution of a signal is a common issue in signal theory [60]. One of the most effective techniques to overcome this issue, frequently used in signal theory but not yet applied to DRT to the best of our knowledge, is the zero-padding technique [61,62], which is advanced in this study to improve the quality of DRT in Tikhonov regularization. The key idea of the zero-padding technique is to extend the experimental frequency domain vector at both ends in the following way:

$$\log_{10}(\boldsymbol{\omega}_{ED}) = \begin{cases} \log_{10}(\boldsymbol{\omega}_{exp}) \\ \log_{10}(\omega_{min}) - k \cdot \Delta\varepsilon \quad \text{with } k = 1, \ldots, Q \quad \text{for } \omega < \omega_{min} \\ \log_{10}(\omega_{max}) + k \cdot \Delta\varepsilon \quad \text{with } k = 1, \ldots, Q \quad \text{for } \omega > \omega_{max} \end{cases} \tag{15}$$

where $\boldsymbol{\omega}_{\mathbf{ED}}$ and $\boldsymbol{\omega}_{\mathbf{exp}}$ are the extended frequency and experimental frequency log-spaced vectors, respectively. The parameter Q is equal to:

$$Q = \lceil N \cdot \xi \rceil \tag{16}$$

where ξ is the extension factor, and the parenthesis indicates the ceiling function, which returns the first integer value following the real value of $N \cdot \xi$. As an example, should the number of experimental frequency points be $N = 100$ and assuming $\xi = 0.2$, the frequency domain is extended both above ω_{max} and below ω_{min} by 20 additional frequencies equally spaced in logarithmic scale by $\Delta\varepsilon$, which is the logarithmic step used for the frequency sweep during the impedance sampling.

After the frequency domain extension, the columns of the matrix **A**, whose elements are calculated according to Eq. (11), are increased to $M = N+2Q$ elements (i.e., the square matrix $\mathbf{A}^{N\times N}$ becomes a non-quadratic matrix $\mathbf{A}^{N\times M}$) and so does the unknown row vector $\boldsymbol{\rho}$, which becomes $\boldsymbol{\rho}_{\mathbf{ED}}$ of size $M \times 1$. The imaginary impedance vector is extended by zero-padding as well and, in order to avoid a degenerate linear system, the final extended matrix $\mathbf{A}_{ED}$ and the zero-padded impedance vector $\mathbf{Z}_{Im\_ED}$ assume the following forms:

$$\boldsymbol{A}_{\boldsymbol{ED}} = \begin{bmatrix} \boldsymbol{A}^{N\times M} \\ \mathbf{0}^{K\times(M-K)}, \vartheta \cdot \boldsymbol{I}^{K\times K} \end{bmatrix} \tag{17}$$

$$\boldsymbol{Z}_{\boldsymbol{Im\_ED}} = \begin{bmatrix} \boldsymbol{Z}_{\boldsymbol{Im}}^{N\times 1} & \mathbf{0}^{K\times 1} \end{bmatrix} \tag{18}$$

where the size $K = (M - N) + M \cdot \xi$, ϑ is the floating-point relative accuracy used by Matlab® (called with the command eps and equal to $\vartheta = 2^{-52} \approx 2.2\cdot10^{-16}$), $0^{K\times(M-K)}$ is the null matrix of size $K \times (M–K)$ and $\boldsymbol{I}$ is the identity matrix. The extended matrix $\mathbf{A}_{ED}$ and the extended vector $\boldsymbol{Z}_{\mathbf{Im\_ED}}$ are introduced in the linear system $\boldsymbol{A}_{\mathbf{ED}}\boldsymbol{\rho}_{\mathbf{ED}} = \boldsymbol{Z}_{\mathbf{Im\_ED}}$, which is solved with Tikhonov regularization to obtain the vector $\boldsymbol{\rho}_{\mathbf{ED}}$, as follows:

$$\min \left\{ \|\boldsymbol{A}_{\boldsymbol{ED}}\boldsymbol{\rho}_{\boldsymbol{ED}} - \boldsymbol{Z}_{\boldsymbol{Im\_ED}}\|^2 + \|\lambda\boldsymbol{\rho}_{\boldsymbol{ED}}\|^2 \right\} \tag{19}$$

Thanks to the damping effect introduced by the zero-padding technique, such a solution $\boldsymbol{\rho}_{\mathbf{ED}}$, whose components $\rho_{ED,j}$ are sorted afterwards and span an extended frequency range, is less affected by the edge errors introduced by the frequency truncation, enabling for a more accurate evaluation of the DRT function compared to the Tikhonov regularization performed on the original Toeplitz matrix **A** in Eq. (13).

The ED-DRT method is released to the electrochemical community as an open-source software in the Supplementary Material.

3. Experimental

A symmetrical solid oxide cell (SOC) half-cell has been used to validate the new DRT method on a real system. Both electrodes were made of porous $La_{0.6}Sr_{0.4}Fe_{0.8}Co_{0.2}O_{3-\delta}$ (LSCF64 – Fuel Cell Materials) deposited by slurry coating on a $Sm_{0.2}Ce_{0.8}O_{2-\delta}$ (SDC – Fuel Cell Materials) electrolyte. The electrolyte was pressed at 4 tons and then sintered at 1500 °C for 5 h. The LSCF powder was mixed in a mortar with α-therpineol (Sigma Aldrich, tech grade 90%) to obtain an ink for the slurry coating. After a symmetrical deposition, the electrodes were sintered at 1100 °C for 2 h in accordance with previous studies [63–65] with a final geometrical area of 0.28 cm^2. This electrochemical system has been chosen because it is well-known and up today it represents one of the most commercially used oxygen-electrode materials in SOC market.

Impedance measurements were carried out with a potentiostat coupled to a frequency response analyzer (Autolab PGSTAT302N). The tests were performed at open circuit voltage, with a perturbation of 10 mV and in a frequency range of 0.01 Hz to 100 kHz. The perturbation of 10 mV was chosen after the evaluation of the stability and linearity of the EIS measurement. The points per decade (ppd) used to sample the system were varied from 2 to 50 ppd.

4. Results and discussion

4.1. Simulated data

The comparison between Tikhonov and ED-DRT algorithms starts considering simulated electrochemical impedance spectroscopy data obtained from equivalent circuit simulations. The circuit takes into account a series of two subcircuits, each one consisting of a resistor (R) in parallel with a constant phase element (Q), that is, $(RQ)_1(RQ)_2$ with $R_1 = 50\ \Omega$, $Q_1 = 0.02$ F $s^{-0.45}$, $n_1 = 0.55$, $R_2 = 2\ \Omega$, $Q_2 = 0.002$ F $s^{-0.05}$, $n_2 = 0.95$. Fig. 2 shows Nyquist and Bode plots for the simulation with 8 ppd in the frequency range of $10^{-2} \div 10^6$ Hz. Several aspects support the choice

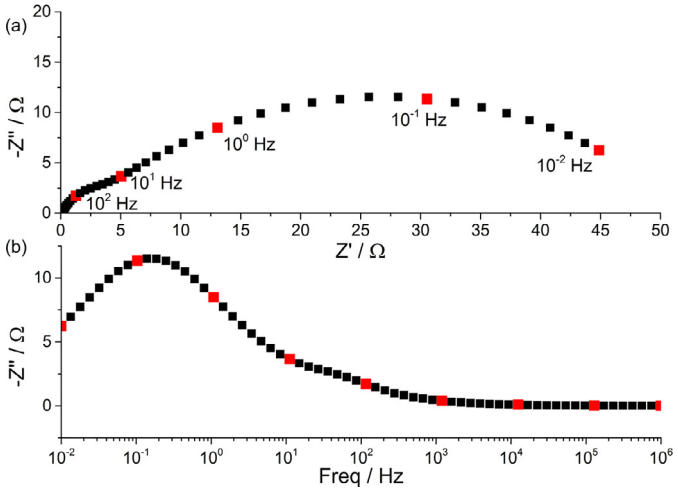

Fig. 2. (a) Nyquist and (b) Bode plots of simulated data with the equivalent circuit $(RQ)_1(RQ)_2$ with $R_1 = 50\ \Omega$, $Q_1 = 0.02$ F $s^{-0.45}$, $n_1 = 0.55$, $R_2 = 2\ \Omega$, $Q_2 = 0.002$ F $s^{-0.05}$, $n_2 = 0.95$, with 8 ppd in the frequency range of $10^{-2} \div 10^{6}$ Hz.

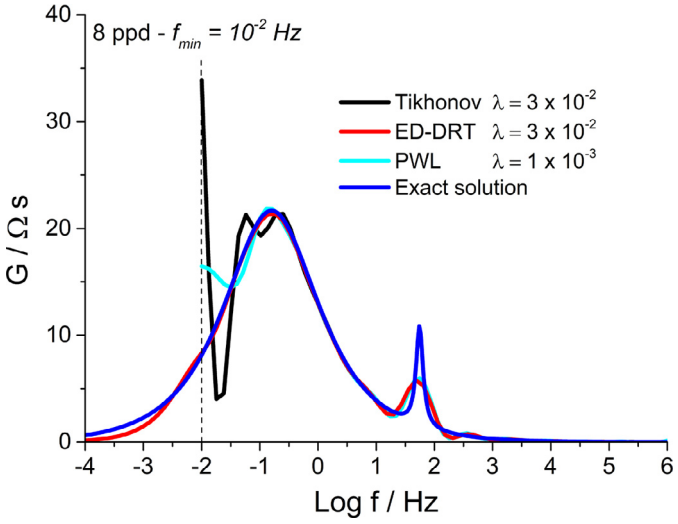

Fig. 3. Distribution of relaxation times for the EIS spectra reported in Fig. 2a obtained using different algorithms with data simulated in the frequency range of $10^{-2} \div 10^{6}$ Hz (8 ppd). (For interpretation of the references to color in this figure, the reader is referred to the web version of this article).

of these parameters: (i) it is quite common to have one phenomenon with a higher resistance than the other one (ii) the characteristic frequencies belong to typical ranges reported in the literature for SOC electrodes (iii) the impedance behaviour described by the equivalent circuit is similar to that reported by the real experimental data, where the impedance spectrum does not close on the real axis of the Nyquist plot at low frequency (see Fig. 2a). This condition, which happens relatively often in real experiments, especially at low temperatures, can represent a source of errors in DRT analysis [46], as reported in Fig. 3. For each subcircuit it is possible to identify the characteristic frequency from Eqs. (20) and (21) (with $k = 1, 2$):

$$C_k = R_k^{(1-n_k)/n_k} Q_k^{1/n_k} \tag{20}$$

$$f_{kC} = 1/(2\pi R_k C_k) \tag{21}$$

which are 0.16 Hz and 53.23 Hz for f_{1C} and f_{2C}, respectively.

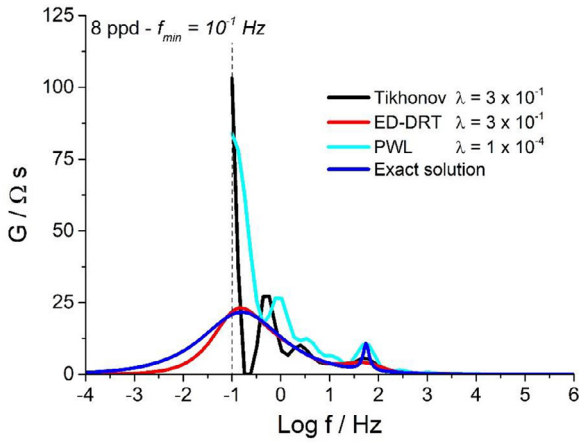

Fig. 4. Distribution of relaxation times for the EIS spectra reported in Fig. 2a obtained using different algorithms with data simulated in the frequency range of $10^{-1} \div 10^{6}$ Hz (8 ppd).

The blue line in Fig. 3 represents the exact DRT solution for the considered equivalent circuit and it is defined as [33]:

$$G(\tau) = \sum_{k=1}^{2} \frac{R_k}{2\pi} \frac{\sin((1-n_k)\pi)}{\cosh(n_k \ln(\tau/\tau_k)) - \cos((1-n_k)\pi)} \tag{22}$$

where τ_k is the characteristic time of each RQ subcircuit ($\tau_k = 1/(2\pi f_{kC})$). The DRT obtained using a pure Tikhonov method (black curve) highly diverges close to the lower frequency limit of 10 mHz. Moreover, the solution shows artefacts in correspondence of f_{1C}, and it could lead to a wrong interpretation of the spectrum as an additional spurious peak shows up at a frequency slightly lower than f_{1C}. The DRT extracted with the piecewise linear (PWL) discretization function of the popular application DRTtools [46] (light blue curve) well identifies both the peaks, while still showing an artefact at the lower frequency limit of 10 mHz. The ED-DRT method (in red), proposed here, provides the best approximation of the ideal DRT, also outside from the frequency range considered in the EIS simulation thanks to the frequency extension, as no artefacts appear for $f < 10^{-2}$ Hz, that is, beyond the lower frequency limit. As such, the ED-DRT method is the only one, among the methods investigated here, which can identify all the processes without any artefacts when the impedance spectrum in the Nyquist plot does not close to the real axis at the lower (and upper too) frequency limit.

To test the reliability of the ED-DRT approach, the second step consists of applying DRT analysis to EIS data in a narrower frequency range, in particular down to 0.1 Hz, which is slightly lower than the characteristic frequency of the first subcircuit ($f_{1C} = 0.16$ Hz). This cut in impedance data is representative of a situation when it would be experimentally difficult or time-consuming collecting EIS data to frequencies low enough to let the Nyquist plot close on the real axis, thus resulting in incomplete spectra. In this case, a strong modification of DRT is obtained with Tikhonov and PWL methods as reported in Fig. 4. This is evident especially for the peak at lower frequency, which is very close (0.16 Hz) to the lower frequency limit of 0.1 Hz. Additional and fake signals are identified in the frequency interval of 0.1–10 Hz, indicating that these algorithms are not suitable to perform DRT when the imaginary component of impedance collected at low frequency bound is not sufficiently close to zero. On the other hand, the result of ED-DRT function (red) remains extremely stable inside the simulated range ($10^{-1} \div 10^{6}$ Hz), with a good identification of both the peaks, and provides a fair approximation of the exact solution in the extended domain part ($f < 10^{-1}$ Hz) where simu-

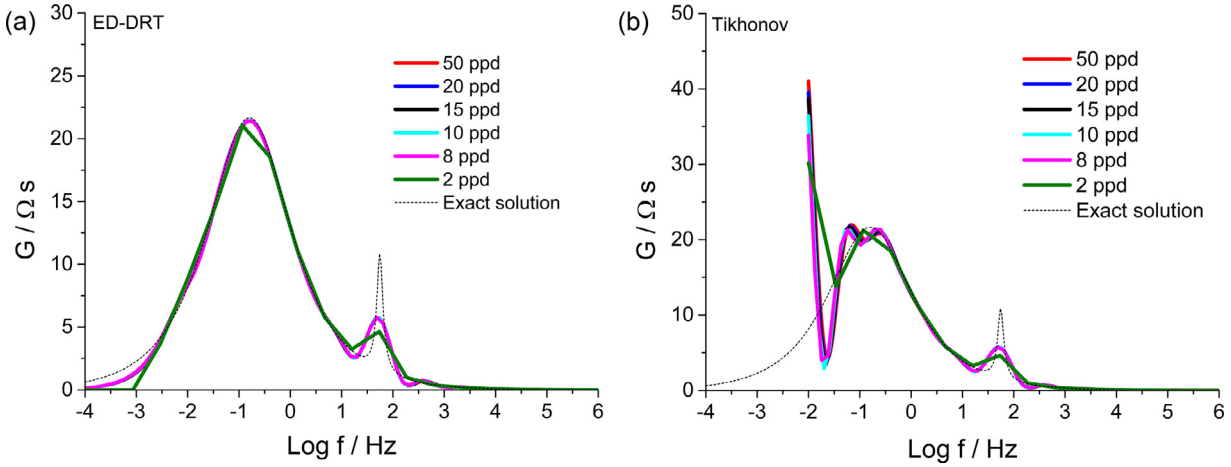

Fig. 5. DRT with (a) ED-DRT and (b) Tikhonov methods for EIS data obtained from equivalent circuit $(RQ)_1(RQ)_2$ with $R_1 = 50\ \Omega$, $Q_1 = 0.02\ F\ s^{-0.45}$, $n_1 = 0.55$, $R_2 = 2\ \Omega$, $Q_2 = 0.002\ F\ s^{-0.05}$, $n_2 = 0.95$ as a function of the number of ppd within the range $10^{-2} \div 10^{6}$ Hz.

lated data were not collected. In this case the main variations are a little increase of the DRT function G close to the main peak value and a steeper slope of the curve at low frequency ($f < 0.1$ Hz) compared to the exact solution. Considering that these modifications occur very close to the frequency threshold of 100 mHz, the quality of DRT remains high for the ED-DRT. The change of the peak at higher frequency (50 Hz) in ED-DRT is ascribable to the variation of the optimal regularization parameter, which increases from 0.03 to 0.4 as the lower bound of frequencies collected increases from 10^{-2} Hz in Fig. 3 to 10^{-1} Hz in Fig. 4, which is in agreement with the influence of the regularization parameter on the sharpness of DRT as well documented in the literature [47,48].

Based on this preliminary analysis a deeper investigation on the robustness of ED-DRT performance has been carried out, comparing the results with the well-known Tikhonov algorithm. The first application is on simulated data, like those presented above, and the influence of the points per decade (ppd) used for the EIS measurements within the frequency range $10^{-2} \div 10^{6}$ Hz. Fig. 5 a-b report the DRT from ED-DRT and Tikhonov methods, respectively. Although both the methods are able to provide information about the characteristic frequency of the involved processes also with only 2 ppd, the application of ED-DRT algorithm increases the quality of the analysis. In fact, moving to a number of ppd closer to that usually used in experimental tests (ppd $\geq$ 8), the DRT from the Tikhonov method not only diverges at the lower frequency limit but also shows artefacts, such as additional peaks, which can lead to a wrong interpretation of impedance data with an overestimation of the number of processes involved in the electrochemical system. In other words, with the Tikhonov regularization method, the quality of DRT effectively worsens as the number of points per decade increases, which is clearly an undesired feature.

On the other hand, the ED-DRT method provides stable results even for EIS data collected with a quite low number of ppd. In addition, the possibility to extend the DRT domain at low frequency, beyond the limit of the impedance data, allows the evaluation of the overall polarization resistance (R_P) with higher accuracy. In fact, the area under the curves reported in Fig. 5 a,b represents the global polarization resistance. The expected R_P value for this simulation is 52 Ω (R_1+R_2), and the most common way to determine this quantity is the difference $R_p = Z'(\omega \to \infty) - Z'(\omega \to 0)$, where Z' is the real part of impedance, usually graphically identified by the two intercepts of the curve with the Z'-axis in the Nyquist plot. In this case, the EIS curve does not intercept the real axis at low frequency unless the EIS frequency range is widened to a lower value (e.g. 10^{-3} Hz); such an extension to collect data at low frequencies is often hard to apply or impractical in a real system. In fact, measuring EIS data at very low frequency is both time consuming and can prejudge the quality of the results because the system must remain stable (i.e., time-invariant) during the whole EIS measurement. This requirement is not always ensured due to temporal variations of the operating conditions or the system itself due to, say, degradation phenomena. Thus, it is necessary to find a method to estimate the global resistance even for incomplete EIS data. The evaluation of R_P from the area under the DRT curve gives a resistance of 47.8 Ω and 50.6 Ω from Tikhonov and ED-DRT, respectively, with relative errors of 8.1 and 2.7% compared to the expected analytical total resistance equal to 52 Ω.

To test the robustness of ED-DRT method, EIS spectra have been simulated with the addition of noise to the impedance data. The noise has been added both to the real and imaginary parts of impedance using the following equation:

$$Z_k^{noise}(\omega) = Z_k(\omega) + \alpha |Z(\omega)| \varphi_k, \quad k = Z' \text{ or } Z'' \tag{23}$$

where $Z_k^{noise}(\omega)$ is the real (Z') or imaginary (Z'') part at angular frequency ω with the noise, $Z_k(\omega)$ is Z' or Z'' simulated without noise, $|Z(\omega)|$ the module of impedance and φ_k is a normally distributed random quantity characterized to have mean (μ) equal to 0 and variance (σ) equal to 1. The parameter α is the noise level, which has been assumed within the interval 0.1÷ 2%. Fig. 6 (a,c,e,g) report the effect of the noise addition on EIS simulation data with a noise level from 0.1 to 2%. Fig. 6 (b,d,f,h) show the Kramers – Kronig test performed using the Linear Kramers – Kronig validity test, a tool developed by the Ivers-Tiffée's group [66]. The residual with 2% of noise (Fig. 6 h) is quite high, especially at low frequencies and shows a random distribution, confirming the random nature of the error purposely introduced in the EIS data.

The change of noise level has a different effect as a function of the ppd for both methods, as shown in Fig. 7 (a–d). Tikhonov method (Fig. 7 c,d) suffers of higher instability, in particular at low ppd, where the peak close to 0.1 Hz shifts significantly as the noise level increases. Increasing the ppd to 50 compensates the negative effect of noise; actually, the accuracy of Tikhonov method in peak detection becomes even better as the noise level increases, resulting in a smoother DRT (Fig. 7 d). Such a counterintuitive trend is a clear limitation for the Tikhonov method and may lead to erroneous conclusions. Suppose one measures the EIS of a system for lower and lower noise levels, for example by increasing the quality of the EIS analyzer and/or the accuracy of flow and temperature controllers. Fig. 7 c,d show that the number of (fictitious) peaks increases as the noise level decreases (compare light blue curve, at

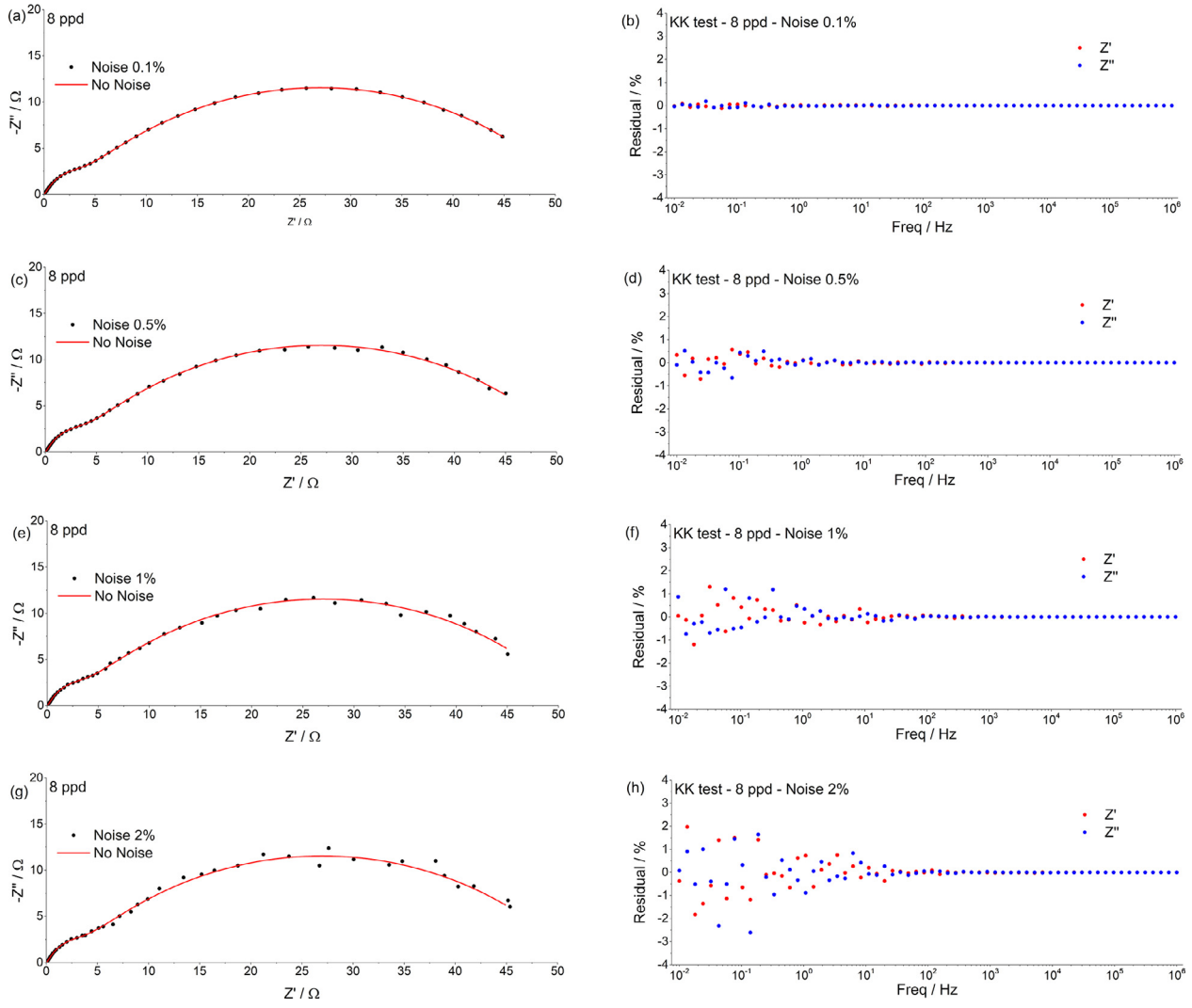

Fig. 6. (a,c,e,g) Nyquist plot of simulated data with equivalent circuit $(RQ)_1(RQ)_2$ with $R_1 = 50\ \Omega$, $Q_1 = 0.02\ F\ s^{-0.45}$, $n_1 = 0.55$, $R_2 = 2\ \Omega$, $Q_2 = 0.002\ F\ s^{-0.05}$, $n_2 = 0.95$, with 8 ppd in the frequency range of $10^{-2} \div 10^{6}$ Hz without noise (red line), and with addition of noise. (b,d,f.h) Corresponding Kramers – Kronig tests. (For interpretation of the references to color in this figure, the reader is referred to the web version of this article).

2 % noise, with black curve, at 0 % noise): this trend may induce one to believe that, after improving the quality of EIS data, additional processes have been identified. However, in reality the EIS spectrum consists of two RQ processes only and the split of the main peak at ca. 0.1 Hz is a consequence of the artefacts generated when the Tikhonov method is applied to spectra that do not close on the real axis at low frequency.

On the other hand, the ED-DRT shows more consistent trends and outperforms the Tikhonov method in all the situations. At 8 ppd, peaks become generally broader as the noise level increases and the minor peak at ca. 50 Hz becomes less distinguishable (Fig. 7 a). Nevertheless, no fictitious peaks arise and the resolution of ED-DRT is comparatively better than what achieved by the Tikhonov method in the same condition, where the minor peak at ca. 50 Hz almost disappears at 2 % level of noise (see light blue curve in Fig. 7 c). By increasing the number of ppd from 8 to 50, the ED-DRT method DRT provides a good and reliable identification of peaks for noise level up to 2 %, with peak resolution worsening monotonically as the noise level increases, especially for the sharp peak at ca. 50 Hz, but without showing additional fictitious signals. In general, Fig. 7 b indicates that even noisy data, which may pass the KK-test as in Fig. 6 h, can be reliably analyzed with ED-DRT by increasing the number of ppd. In addition, as shown in detail in the supplementary material, the ED-DRT algorithm maintains the ability to provide a reliable DRT even operating with EIS data cut at 100 mHz in presence of noise.

4.2. Experimental data

The first application of ED-DRT method on real data is performed on a LSCF electrode on SDC electrolyte as reported in the experimental section. The analysis is carried out considering data in similar conditions of simulated ones where the imaginary component of impedance at the lower frequency bound is far from zero, so that the impedance curve does not intersect the real axis in the Nyquist plot. Experimental results at 400 °C are reported in Fig. 8, with the corresponding Kramers- Kronig analysis. The development of a tool able to provide a reliable interpretation of data also at low temperature is fundamental for a clear understanding of which phenomena dominate electrochemical systems.

The electrochemical system has been investigated, repeating the impedance measurements at different ppd in the range of $2 \div 50$ ppd. The experimental EIS curve shape is reported in Fig. 8 for data collected at 50 ppd, which shows one main arc at a lower frequency and one smaller and depressed shoulder at a higher frequency.

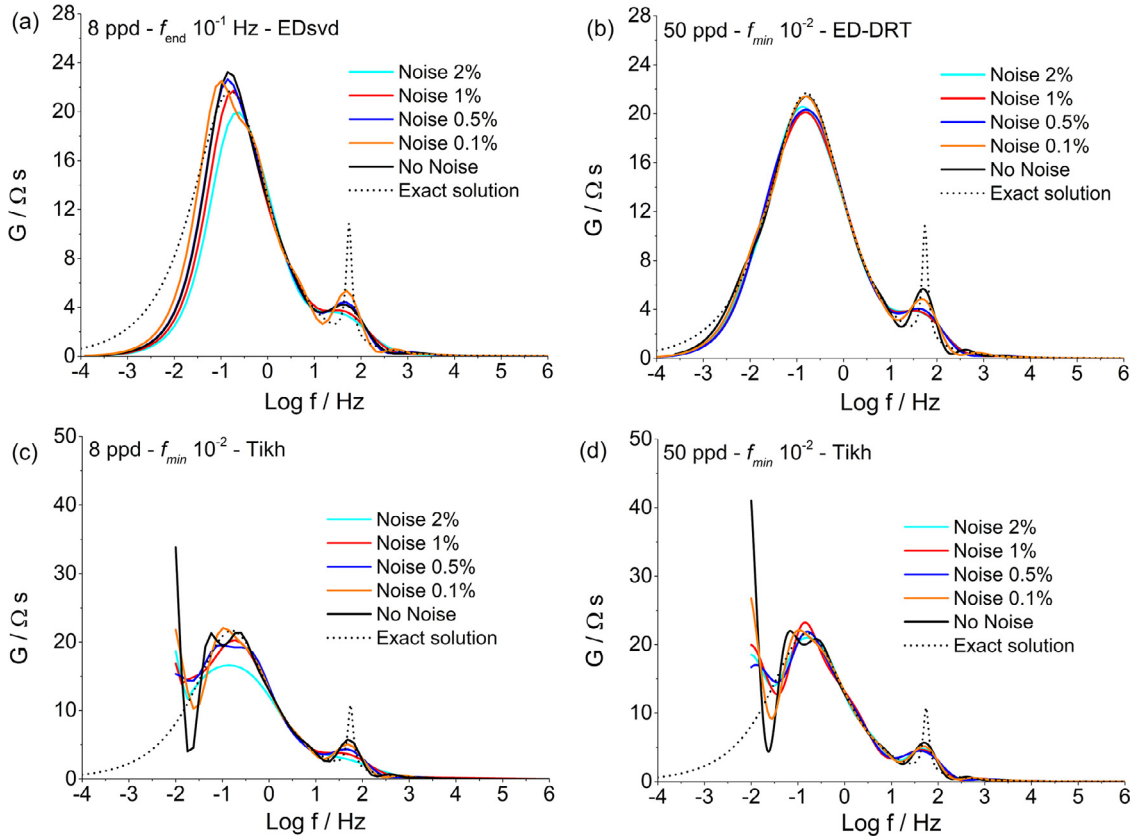

Fig. 7. DRT results obtained with (a,b) ED-DRT and (c,d) Tikhonov method at different ppd (a,c) 8 ppd and (b,d) 50 ppd as a function of noise applied to the EIS simulation. Regularization parameters are in a range of 1×10^{-2}- 6×10^{-1} (a complete list of regularization parameters is reported in Table S.1 of Supporting Material). (For interpretation of the references to color in this figure, the reader is referred to the web version of this article).

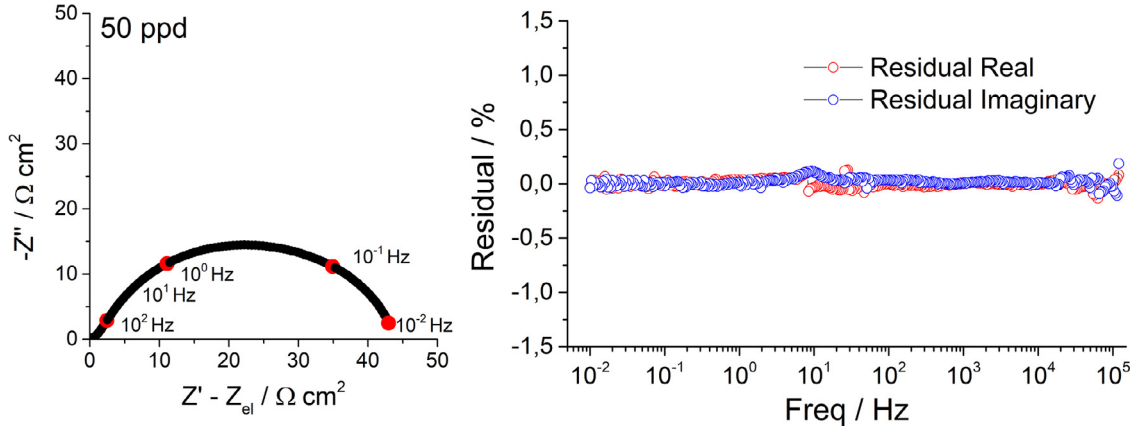

Fig. 8. Experimental EIS for half-cell of LSCF electrode deposited on a SDC electrolyte at 400 °C, OCV and 21% O_2 and the residual of Kramers – Kronig test.

Fig. 9 (a–d) presents all the DRT results obtained with ED-DRT and Tikhonov methods at different ppd and different end frequency limits. As observed before with the simulated data, also in this case, 2 ppd are sufficient only to identify an interval, which includes the characteristic frequency of the main process. Nevertheless, in order to refine DRT analysis, a threshold of 8 ppd is necessary as demonstrated before: beyond this value, both methods provide a peak close to 0.4 Hz, that remains stable even at higher ppd.

The more relevant difference between ED-DRT and Tikhonov method is located close to 10 mHz; the former produces a descending curve thanks to DRT data extension, while the latter suffers again from the divergent behaviour. This difference is emphasized when the EIS data are cut at 100 mHz (Fig. 9 b–d), and the *G* function in the Tikhonov algorithm rises a lot. A secondary effect of the cutting of frequency domain is the disappearance of the shoulder visible in Fig. 9 a–c around 100 mHz. Despite the loss of this information, the ED-DRT method remains stable and reliable also in these conditions for the estimation of global R_P. Indeed, the mean area under the DRT curves in case (a) and (b) is 43.8 Ω cm^2 and 43.9 Ω cm^2, respectively.

Going into more detail about the DRT results, a comparison with equivalent circuit modelling (ECM) is proposed in Fig. 10 (a,b) that reports the EIS measurement at 400 °C and OCV conditions with data collected in the frequency range of $10^{-2} \div 10^{6}$ Hz with 50 ppd. The equivalent circuit chosen is able to fit properly experi-

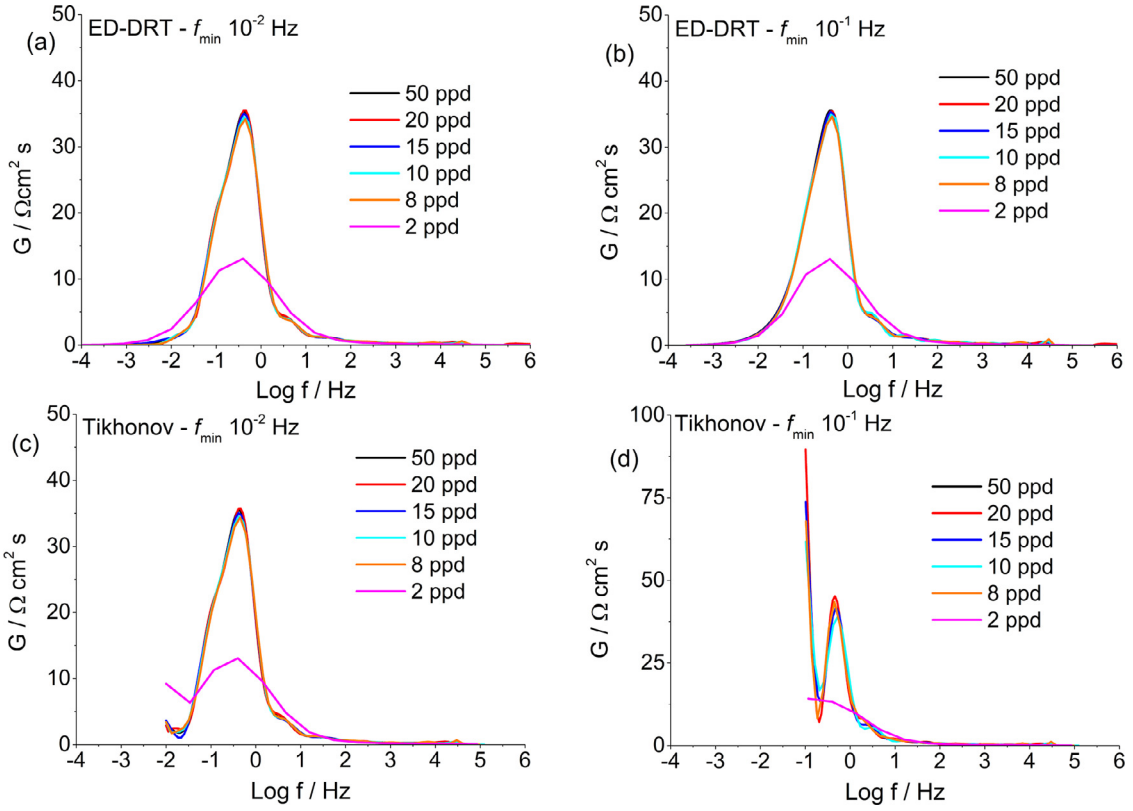

Fig. 9. DRT results obtained with (a,b) ED-DRT and (c,d) Tikhonov method for a LSCF64 electrode on SDC electrolyte at 400 °C, OCV and 21% O_2. Fig. (a) and (c) are related with EIS data collected up to 10^{-2} Hz, (b) and (d) up to 10^{-1} Hz.

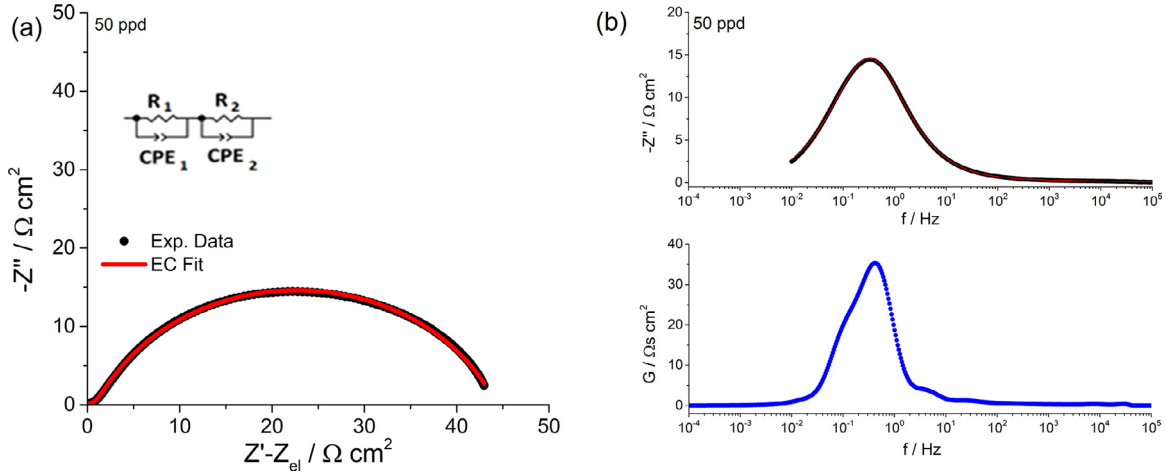

Fig. 10. (a) EIS curve at 400 °C, OCV, 21% O_2 for LSCF64 electrode on SDC electrolyte overlaps to equivalent circuit (EC) fit. (b) (up) Bode plot and (down) ED-DRT curve.

mental data. The resistances associated with two processes R_1 and R_2 have values of 42.98 Ω cm^2 and 1.46 Ω cm^2, respectively. Then, the global R_P is 44.44 Ω cm^2 very close to the resistance evaluated through the ED-DRT method, with a 1.2% relative difference. The reliability of the extended method is also confirmed by the identification of the characteristic frequency of the processes. The low frequency process is identified at 0.38 Hz and 0.32 Hz by DRT peak and equivalent circuit model, respectively. Moreover, the results of ECM can also justify the tail, which follows the main peak in DRT curve (which is not exactly symmetric), between 10 and 100 mHz (see Fig. 10 b). In fact, the CPE parameter n_1 is equal to 0.75 from ECM: although such a value does not describe a pure Gerischer behavior ($n = 0.5$), it suggests that both capacity and diffusive phenomena occur simultaneously [22], thus leading to a broader frequency dispersion than a pure capacitive phenomenon [43]. Such qualitative information from equivalent circuit analysis provides an additional indication on the quality of the ED-DRT method, which does capture a non-symmetric signal between 10 and 100 mHz as shown in Fig. 10 b.

5. Conclusion

This study advanced a procedure, named Extended Domain-Distribution of Relaxation Times (ED-DRT), capable of overcoming some limitations of the classical Tikhonov regularization method. The ED-DRT method is tested for the analysis of the Distribution of Relaxation Times (DRT), especially for EIS data which are incomplete at the frequency bounds as when the imaginary component

of impedance does not approach zero (i.e., the spectrum does not close on the real axis in the Nyquist plot). The ED-DRT approach relies on a convenient extension of the frequency values beyond the range of frequencies collected experimentally using the zero-padding method.

The ED-DRT was compared against the classical Tikhonov approach for EIS data artificially generated with equivalent circuits as well as with experimental data of a real electrochemical system, namely a solid oxide cell electrode tested at low temperature. The proposed refinement of the original DRT analysis was shown to be a promising upgrade of the traditional algorithm due to the capability of the zero padding-based algorithm to provide a reliable DRT and to resolve peak processes when the characteristic frequency of one of processes is close to the cutoff frequency of the collected range of data. On the contrary, the Tikhonov approach diverged in such conditions, negatively affecting the quality of DRT resolution even for processes relatively far from the cutoff frequency, showing spurious peaks and fictitious signals. In addition, the robustness of the ED-DRT against increased levels of noise and reduced number of points per decade was proved. In general, the quality of peak resolution resulting from the application of the ED-DRT increased as the level of noise decreased or the number of points of decade increased; instead, opposite trends resulted from the application of the Tikhonov method, which is obviously an undesired and possibly misleading feature of the latter. Finally, the application of the ED-DRT on experimental EIS data revealed that reliable information on the nature of processes as well as accurate estimation of process resistances can be obtained as confirmed by the comparison with equivalent circuit modeling.

In summary, the ED-DRT represents a robust approach for DRT analysis, outperforming the classical Tikhonov regularization especially for incomplete EIS spectra. Moreover, the ED-DRT method is released to the electrochemical community as an open-source software in the Supplementary Material.

Declaration of Competing Interest

None

Supplementary materials

Supplementary material associated with this article can be found, in the online version, at doi:10.1016/j.electacta.2021.138916.

References

[1] J.R.M.E. Barsoukov, Impedance Spectroscopy: Theory, Experiment and Applications, 2nd ed., John Wiley & Sons, 2005.

[2] C. Gabrielli, Once upon a time there was EIS, Electrochim. Acta 331 (2020) 135324, doi:10.1016/j.electacta.2019.135324.

[3] D.D. Macdonald, Reflections on the history of electrochemical impedance spectroscopy, Electrochim. Acta 51 (2006) 1376–1388, doi:10.1016/j.electacta.2005.02.107.

[4] A. Nechache, A. Mansuy, M. Petitjean, J. Mougin, F. Mauvy, B.A. Boukamp, M. Cassir, A. Ringuedé, Diagnosis of a cathode-supported solid oxide electrolysis cell by electrochemical impedance spectroscopy, Electrochim. Acta 210 (2016) 596–605, doi:10.1016/j.electacta.2016.05.014.

[5] M. Cimenti, A.C. Co, V.I. Birss, J.M. Hill, Distortions in electrochemical impedance spectroscopy measurements using 3-electrode methods in SOFC. I – effect of cell geometry, Fuel Cell 7 (2007) 364–376, doi:10.1002/fuce.200700019.

[6] A.R. Thompson, A.V. Call, D.J. Cumming, D.C. Sinclair, R.H. Elder, Electrochemical impedance spectroscopy data from solid oxide cells undergoing co-electrolysis: the influence of rig inductance, ECS Trans 68 (2015) 3417.

[7] D. Klotz, A. Weber, E. Ivers-Tiffée, Practical guidelines for reliable electrochemical characterization of solid oxide fuel cells, Electrochim. Acta 227 (2017) 110–126, doi:10.1016/j.electacta.2016.12.148.

[8] J. Jamnik, J. Maier, Treatment of the impedance of mixed conductors equivalent circuit model and explicit approximate solutions, J. Electrochem. Soc. 146 (1999) 4183–4188, doi:10.1149/1.1392611.

[9] W. Lai, S.M. Haile, Impedance spectroscopy as a tool for chemical and electrochemical analysis of mixed conductors: a case study of ceria, J. Am. Ceram. Soc. 88 (2005) 2979–2997, doi:10.1111/j.1551-2916.2005.00740.x.

[10] D.A. Harrington, P. van den Driessche, Mechanism and equivalent circuits in electrochemical impedance spectroscopy, Electrochim. Acta 56 (2011) 8005–8013, doi:10.1016/j.electacta.2011.01.067.

[11] A. Bertei, G. Arcolini, J.P. Ouweltjes, Z. Wuillemin, P. Piccardo, C. Nicolella, Physically-based deconvolution af impedance spectra: interpretation, fitting and validation of a numerical model for lanthanum strontium cobalt ferrite-based solid oxide fuel cells, Electrochim. Acta 208 (2016) 129–141, doi:10.1016/j.electacta.2016.04.181.

[12] A. Bertei, M.P. Carpanese, D. Clematis, A. Barbucci, M.Z. Bazant, C. Nicolella, Understanding the electrochemical behavior of LSM-based SOFC cathodes. Part II - Mechanistic modelling and physically-based interpretation, Solid State Ion. 303 (2017) 181–190, doi:10.1016/j.ssi.2016.09.028.

[13] S.J. Cooper, A. Bertei, D.P. Finegan, N.P. Brandon, Simulated impedance of diffusion in porous media, Electrochim. Acta 251 (2017) 681–689, doi:10.1016/j.electacta.2017.07.152.

[14] A. Donazzi, G. Cordaro, A. Baricci, Z.B. Ding, M. Maestri, A detailed kinetic model for the reduction of oxygen on LSCF-GDC composite cathodes, Electrochim. Acta 335 (2020) 135620, doi:10.1016/j.electacta.2020.135620.

[15] A. Donazzi, S. De Pascali, F. Garavaglia, M. Bracconi, A quasi 2D model for the interpretation of impedance and polarization of a planar solid oxide fuel cell with interconnects, Electrochim. Acta 365 (2021) 137346, doi:10.1016/j.electacta.2020.137346.

[16] S. Gewies, W.G. Bessler, Physically based impedance modeling of Ni/YSZ cermet anodes, J. Electrochem. Soc. 155 (2008) B937–B952, doi:10.1149/1.2943411.

[17] A. Häffelin, J. Joos, M. Ender, A. Weber, E. Ivers-Tiffée, Time-dependent 3D impedance model of mixed-conducting solid oxide fuel cell cathodes, J. Electrochem. Soc. 160 (2013) F867–F876, doi:10.1149/2.093308jes.

[18] H. Zhu, R.J. Kee, Modeling electrochemical impedance spectra in SOFC button cells with internal methane reforming, J. Electrochem. Soc. 153 (2006) A1765–A1772, doi:10.1149/1.2220065.

[19] B. Hirschorn, M.E. Orazem, B. Tribollet, V. Vivier, I. Frateur, M. Musiani, Determination of effective capacitance and film thickness from constant-phase-element parameters, Electrochim. Acta 55 (2010) 6218–6227, doi:10.1016/j.electacta.2009.10.065.

[20] J.B. Jorcin, M.E. Orazem, N. Pébère, B. Tribollet, CPE analysis by local electrochemical impedance spectroscopy, Electrochim. Acta 51 (2006) 1473–1479, doi:10.1016/j.electacta.2005.02.128.

[21] B.A. Boukamp, Electrochemical impedance spectroscopy in solid state ionics: recent advances, Solid State Ion. 169 (2004) 65–73, doi:10.1016/j.ssi.2003.07.002.

[22] B.A. Boukamp, H.J.M. Bouwmeester, Interpretation of the gerischer impedance in solid state ionics, Solid State Ion. 157 (2003) 29–33, doi:10.1016/S0167-2738(02)00185-6.

[23] A. Lasia, Electrochemical Impedance Spectroscopy and its Applications, Springer, 2014.

[24] G. Paasch, K. Micka, P. Gersdorf, Theory of the electrochemical impedance of macrohomogeneous porous electrodes, Electrochim. Acta 38 (1993) 2653–2662, doi:10.1016/0013-4686(93)85083-B.

[25] U. Tröltzsch, O. Kanoun, Generalization of transmission line models for deriving the impedance of diffusion and porous media, Electrochim. Acta 75 (2012) 347–356, doi:10.1016/j.electacta.2012.05.014.

[26] F.S. Baumann, J. Fleig, H.U. Habermeier, J. Maier, Impedance spectroscopic study on well-defined (La,Sr)(Co,Fe)$O_{3-\delta}$ model electrodes, Solid State Ion. 177 (2006) 1071–1081, doi:10.1016/j.ssi.2006.02.045.

[27] M. Kubicek, T.M. Huber, A. Welzl, A. Penn, G.M. Rupp, J. Bernardi, M. Stöger-Pollach, H. Hutter, J. Fleig, Electrochemical properties of $La_{0.6}Sr_{0.4}CoO_{3-\delta}$ thin films investigated by complementary impedance spectroscopy and isotope exchange depth profiling, Solid State Ion. 256 (2014) 38–44, doi:10.1016/j.ssi.2013.12.016.

[28] W.G. Bessler, S. Gewies, M. Vogler, A new framework for physically based modeling of solid oxide fuel cells, Electrochim. Acta 53 (2007) 1782–1800, doi:10.1016/j.electacta.2007.08.030.

[29] M.P. Eschenbach, R. Coulon, A.A. Franco, J. Kallo, W.G. Bessler, Multi-scale simulation of fuel cells: from the cell to the system, Solid State Ion. 192 (2011) 615–618, doi:10.1016/j.ssi.2010.06.041.

[30] A. Leonide, B. Rüger, A. Weber, W.A. Meulenberg, E. Ivers-Tiffée, Impedance study of alternative (La,Sr)FeO[sub $_{3-\delta}$] and (La,Sr)(Co,Fe)O[sub $_{3-\delta}$] MIEC cathode compositions, J. Electrochem. Soc. 157 (2010) B234, doi:10.1149/1.3265473.

[31] T. Ramos, M. Søgaard, M.B. Mogensen, Electrochemical characterization of Ni/ScYSZ Electrodes as SOFC anodes, J. Electrochem. Soc. 161 (2014) F434–F444, doi:10.1149/2.045404jes.

[32] M. Saccoccio, T.H. Wan, C. Chen, F. Ciucci, Optimal regularization in distribution of relaxation times applied to electrochemical impedance spectroscopy: ridge and lasso regression methods - a theoretical and experimental study, Electrochim. Acta 147 (2014) 470–482, doi:10.1016/j.electacta.2014.09.058.

[33] B.A. Boukamp, Fourier transform distribution function of relaxation times; application and limitations, Electrochim. Acta 154 (2015) 35–46, doi:10.1016/j.electacta.2014.12.059.

[34] F. Ciucci, C. Chen, Analysis of electrochemical impedance spectroscopy data using the distribution of relaxation times: a bayesian and hierarchical bayesian approach, Electrochim. Acta 167 (2015) 439–454, doi:10.1016/j.electacta.2015.03.123.

[35] A. Flura, C. Nicollet, S. Fourcade, V. Vibhu, A. Rougier, J.M. Bassat, J.C. Grenier, Identification and modeling of the oxygen gas diffusion impedance in SOFC porous electrodes: application to $Pr_2NiO_{4+\delta}$, Electrochimica Acta 174 (2015) 1030–1040, doi:10.1016/j.electacta.2015.06.084.

[36] M. Schönleber, E. Ivers-Tiffée, The distribution function of differential capacity as a new tool for analyzing the capacitive properties of Lithium-Ion batteries, Electrochem. Commun. 61 (2015) 45–48, doi:10.1016/j.elecom.2015.09.024.
[37] Y. Zhang, Y. Chen, M. Yan, F. Chen, Reconstruction of relaxation time distribution from linear electrochemical impedance spectroscopy, J. Power Source 283 (2015) 464–477, doi:10.1016/j.jpowsour.2015.02.107.
[38] B.A. Boukamp, A. Rolle, Analysis and application of distribution of relaxation times in solid state ionics, Solid State Ion. 302 (2017) 12–18, doi:10.1016/j.ssi.2016.10.009.
[39] E. Ivers-Tiffée, A. Weber, Evaluation of electrochemical impedance spectra by the distribution of relaxation times, J. Ceram. Soc. Jpn. 125 (2017) 193–201, doi:10.2109/jcersj2.16267.
[40] A. Weiß, S. Schindler, S. Galbiati, M.A. Danzer, R. Zeis, Distribution of relaxation times analysis of high-temperature PEM fuel cell impedance spectra, Electrochim. Acta 230 (2017) 391–398, doi:10.1016/j.electacta.2017.02.011.
[41] B.A. Boukamp, A. Rolle, Use of a distribution function of relaxation times (DFRT) in impedance analysis of SOFC electrodes, Solid State Ion. 314 (2018) 103–111, doi:10.1016/j.ssi.2017.11.021.
[42] J. Song, M.Z. Bazant, Electrochemical impedance imaging *via* the distribution of diffusion times, Phys. Rev. Lett. 120 (2018) 116001, doi:10.1103/PhysRevLett.120.116001.
[43] P. Caliandro, A. Nakajo, S. Diethelm, J. Van herle, Model-assisted identification of solid oxide cell elementary processes by electrochemical impedance spectroscopy measurements, J. Power Source 436 (2019) 226838, doi:10.1016/j.jpowsour.2019.226838.
[44] D. Clematis, S. Presto, M.P. Carpanese, A. Barbucci, F. Deganello, L.F. Liotta, C. Aliotta, M. Viviani, Distribution of relaxation times and equivalent circuits analysis of $Ba_{0.5}Sr_{0.5}Co_{0.8}Fe_{0.2}O_{3-\delta}$, Catalysts 9 (2019) 441.
[45] A. Bertei, E. Ruiz-Trejo, F. Tariq, V. Yufit, A. Atkinson, N.P. Brandon, Validation of a physically-based solid oxide fuel cell anode model combining 3D tomography and impedance spectroscopy, Int. J. Hydrog. Energy 41 (2016) 22381–22393, doi:10.1016/j.ijhydene.2016.09.100.
[46] T.H. Wan, M. Saccoccio, C. Chen, F. Ciucci, Influence of the discretization methods on the distribution of relaxation times deconvolution: implementing radial basis functions with DRTtools, Electrochim. Acta 184 (2015) 483–499, doi:10.1016/j.electacta.2015.09.097.
[47] N. Schlüter, S. Ernst, U. Schröder, Finding the optimal regularization parameter in distribution of relaxation times analysis, ChemElectroChem 6 (2019) 6027–6037, doi:10.1002/celc.201901863.
[48] A.L. Gavrilyuk, D.A. Osinkin, D.I. Bronin, The use of tikhonov regularization method for calculating the distribution function of relaxation times in impedance spectroscopy, Russ. J. Electrochem. 53 (2017) 575–588, doi:10.1134/s1023193517060040.
[49] Y. Zhang, Y. Chen, M. Li, M. Yan, M. Ni, C. Xia, A high-precision approach to reconstruct distribution of relaxation times from electrochemical impedance spectroscopy, J. Power Source 308 (2016) 1–6, doi:10.1016/j.jpowsour.2016.01.067.
[50] H. Schichlein, A.C. Müller, M. Voigts, A. Krügel, E. Ivers-Tiffée, Deconvolution of electrochemical impedance spectra for the identification of electrode reaction mechanisms in solid oxide fuel cells, J. Appl. Electrochem. 32 (2002) 875–882, doi:10.1023/a:1020599525160.
[51] R.L. Van Meirhaeghe, E.C. Dutoit, F. Cardon, W.P. Gomes, On the application of the kramers-kronig relations to problems concerning the frequency dependence of electrode impedance, Electrochim. Acta 20 (1975) 995–999, doi:10.1016/0013-4686(75)85062-6.
[52] H. Sumi, H. Shimada, Y. Yamaguchi, T. Yamaguchi, Y. Fujishiro, Degradation evaluation by distribution of relaxation times analysis for microtubular solid oxide fuel cells, Electrochim. Acta 339 (2020) 135913, doi:10.1016/j.electacta.2020.135913.
[53] D. Calvetti, S. Morigi, L. Reichel, F. Sgallari, Tikhonov regularization and the L-curve for large discrete ill-posed problems, J. Comput. Appl. Math. 123 (2000) 423–446, doi:10.1016/S0377-0427(00)00414-3.
[54] S. Dierickx, A. Weber, E. Ivers-Tiffée, How the distribution of relaxation times enhances complex equivalent circuit models for fuel cells, Electrochimica Acta 355 (2020) 136764, doi:10.1016/j.electacta.2020.136764.
[55] A. Kežionis, E. Kazakevičius, Some features of the analysis of broadband impedance data using distribution of relaxation times, Electrochim. Acta 349 (2020) 136379, doi:10.1016/j.electacta.2020.136379.
[56] P.C. Hansen, D.P. O'Leary, The use of the L-curve in the regularization of discrete ill-posed problems, SIAM J. Sci. Comput. 14 (1993) 1487–1503, doi:10.1137/0914086.
[57] R.M. Gray, Toeplitz and circulant matrices: a review, Found. Trend. Commun. Inf. Theory 2 (2006) 155–239, doi:10.1561/0100000006.
[58] P.C. Hansen, Deconvolution and regularization with toeplitz matrices, Numer. Algorithm. 29 (2002) 323–378, doi:10.1023/a:1015222829062.
[59] F. Aghdasi, R.K. Ward, Reduction of boundary artifacts in image restoration, Trans. Img. Proc. 5 (1996) 611–618, doi:10.1109/83.491337.
[60] R. Seeber, A. Ulrici, Analog and digital worlds: Part 1. signal sampling and fourier transform, ChemTexts 2 (2016) 18, doi:10.1007/s40828-016-0037-1.
[61] P. Castiglioni, Padding Zero, Wiley StatsRef: Statistics Reference Online (2014), https://doi.org/10.1002/9781118445112.stat05551.
[62] I. Domuta, T.P. Palade, DFT Sliding, Zero Padding, in: Proceedings of the 42nd International Conference on Telecommunications and Signal Processing (TSP), 2019, pp. 154–157.
[63] D. Clematis, A. Barbucci, S. Presto, M. Viviani, M.P. Carpanese, Electrocatalytic activity of perovskite-based cathodes for solid oxide fuel cells, Int. 6J. Hydrog. Energy 44 (2019) 6212–6222, doi:10.1016/j.ijhydene.2019.01.128.
[64] A. Giuliano, M.P. Carpanese, D. Clematis, M. Boaro, A. Pappacena, F. Deganello, L.F. Liotta, A. Barbucci, Infiltration, overpotential and ageing effects on cathodes for solid oxide fuel cells: $La_{0.6}Sr_{0.4}Co_{0.2}Fe_{0.8}O_{3-\delta}$ versus $Ba_{0.5}Sr_{0.5}Co_{0.8}Fe_{0.2}O_{3-\delta}$, J. Electrochem. Soc. 164 (2017) F3114–F3122, doi:10.1149/2.0161710jes.
[65] A. Giuliano, M.P. Carpanese, M. Panizza, G. Cerisola, D. Clematis, A. Barbucci, Characterisation of $La_{0.6}Sr_{0.4}Co_{0.2}Fe_{0.8}O_{3-\delta}$ – $Ba_{0.5}Sr_{0.5}Co_{0.8}Fe_{0.2}O_{3-\delta}$ composite as cathode for solid oxide fuel cells, Electrochim. Acta 240 (2017) 258–266, doi:10.1016/j.electacta.2017.04.079.
[66] M. Schönleber, D. Klotz, E. Ivers-Tiffée, A method for improving the robustness of linear kramers-kronig validity tests, Electrochim. Acta 131 (2014) 20–27, doi:10.1016/j.electacta.2014.01.034.

Update

Electrochimica Acta

Volume 394, Issue , 20 October 2021, Page

DOI: https://doi.org/10.1016/j.electacta.2021.139092

Electrochimica Acta 394 (2021) 139092

Contents lists available at ScienceDirect

Electrochimica Acta

journal homepage: www.elsevier.com/locate/electacta

Corrigendum

Corrigendum to "On the stabilization and extension of the Distribution of Relaxation Times analysis" [Electrochimica Acta 391 (2021) 138916]

Davide Clematis[a,*,**], Tommaso Ferrari[b,**], Antonio Bertei[b,***], Antonio Maria Asensio[a], Maria Paola Carpanese[a,c], Cristiano Nicolella[b], Antonio Barbucci[a,c]

[a] Department of Civil, Chemical and Environmental Engineering (DICCA), University of Genoa, Via all'Opera Pia 15, 16145 Genova, Italy
[b] Department of Civil and Industrial Engineering (DICI), University of Pisa, Largo Lucio Lazzarino 2, 56126 Pisa, Italy
[c] Institute of Condensed Matter Chemistry and Technology for Energy, National Research Council (CNR-ICMATE), Via De Marini 6, 16149 Genova, Italy

The authors regret to inform that in the final online article the supporting information contains a wrong Matlab® App Installer. We include the correct ED-DRT Matlab® application.

The authors would like to apologise for any inconvenience caused.

Supplementary materials

Supplementary data associated with this article can be found, in the online version, at doi:10.1016/j.electacta.2021.139092.

DOI of original article: 10.1016/j.electacta.2021.138916
* Corresponding author.
** These two authors contributed equally to the work.
*** Co-corresponding author.
E-mail addresses: davide.clematis@edu.unige.it (D. Clematis), antonio.bertei@unipi.it (A. Bertei).

https://doi.org/10.1016/j.electacta.2021.139092